Layer-by-Layer Graphene/TCNQ Stacked Films as Conducting Anodes for Organic Solar Cells

Chang-Lung Hsu,[†] Cheng-Te Lin,[‡] Jen-Hsien Huang,[§] Chih-Wei Chu,[§] Kung-Hwa Wei,[†,*] and Lain-Jong Li[‡,*]

[†]Department of Material Science and Engineering, National Chiao Tung University, Hsinchu 300, Taiwan, and [‡]Institute of Atomic and Molecular Sciences and [§]Research Center for Applied Sciences, Academia Sinica, Taipei 11529, Taiwan

ABSTRACT

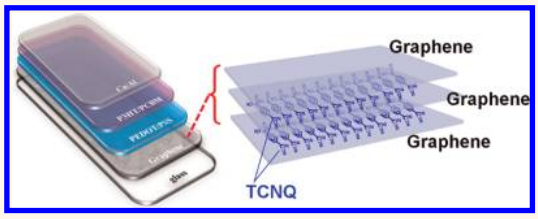

Large-area graphene grown by chemical vapor deposition (CVD) is a promising candidate for transparent conducting electrode applications in flexible optoelectronic devices such as light-emitting diodes or organic solar cells. However, the power conversion efficiency (PCE) of the polymer photovoltaic devices using a pristine CVD graphene anode is still not appealing due to its much lower conductivity than that of conventional indium tin oxide. We report a layer-by-layer molecular doping process on graphene for forming sandwiched graphene/tetracyanoquinodimethane (TCNQ)/graphene stacked films for polymer solar cell anodes, where the TCNQ molecules (as p-dopants) were securely embedded between two graphene layers. Poly(3-hexylthiophene)/phenyl-C61-butyric acid methyl ester (P3HT/PCBM) bulk heterojunction polymer solar cells based on these multilayered graphene/TCNQ anodes are fabricated and characterized. The P3HT/PCBM device with an anode structure composed of two TCNQ layers sandwiched by three CVD graphene layers shows optimum PCE (~2.58%), which makes the proposed anode film quite attractive for next-generation flexible devices demanding high conductivity and transparency.

KEYWORDS: graphene anodes · transparent conducting electrodes · organic solar cell · organic photovoltaic cell · layer-by-layer · doping · TCNQ

Organic photovoltaic devices have attracted much attention in both scientific and application-oriented research due to their unique features including light weight, high bendability, low cost, and compatibility with flexible electronic fabrication processes.[1−9] In these devices, doped metal oxides such as tin-doped indium oxide (ITO) and fluorine-doped tin oxide have been predominantly used as the transparent conducting electrodes.[10] The use of such materials as electrodes may be problematic for organic electronic devices due to the limited indium source on earth and the susceptibility of ion diffusion to organic active layers, which shortens the lifetime of these devices. Moreover, the low stability in acid and lack of bendability of the ITO electrodes hinder their applications in organic electronics. Meanwhile, new electronic devices including touch screens, flexible displays, printable electronics, and solid-state lighting require a more flexible anode material.[11] Carbon nanotube networks,[12−17] reduced graphene oxides,[18−25] and large-area graphene films synthesized by chemical vapor deposition (CVD)[26−30] are considered as promising materials for transparent conducting electrodes. The two-dimensional CVD graphene layers, with superior electrical conductivity and the potential for large-area fabrication, have been developed for many applications, such as field-effect transistors,[31−33] sensors,[34,35] memory devices,[36] and electrodes for light emitting,[37] photodetectors,[38] electrochromic[39] or solar cell devices.[1−9] Many efforts have been devoted to studying the possibility of replacing ITO with graphene layers.[1−5] The enhancement of graphene conductivity to a level comparable with the conductivity of ITO remains as one of the major challenges for utilizing graphene electrodes for organic optoelectronic devices. To reduce the resistance of CVD graphene, various methods for increasing hole carrier concentration in graphene have been reported, including acid, molecule, and Au doping.[30,40−42] In particular, it has been reported that stacking graphene multilayers enhances the extrinsic conductivity, and the power conversion efficiency (PCE) of poly(3-hexylthiophene)/phenyl-C61-butyric acid methyl ester (P3HT/PCBM) devices with the acid-doped multilayer graphene anodes is 1.6−2.5% after optimization of the interface between the graphene anodes and the hole-trapping layer.[43] However, these acid dopants could

* Address correspondence to lanceli@gate.sinica.edu.tw, khwei@mail.nctu.edu.tw.

Received for review February 8, 2012 and accepted May 26, 2012.

Published online May 26, 2012
10.1021/nn301721q

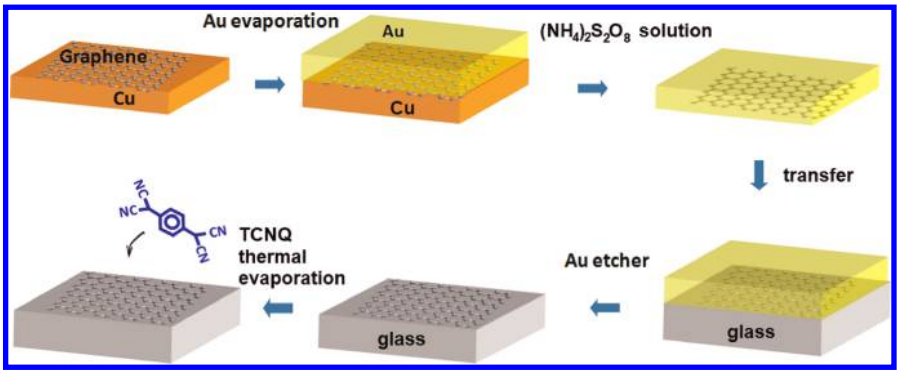

Figure 1. Schematic illustration for the Au-assisted transfer process of graphene. A layer of Au metal was deposited on top of as-synthesized graphene on Cu foils. After the removal of Cu foils by a Cu etcher, $(NH_4)S_2O_8$ solution, the Au-protected graphene was transferred onto a glass substrate followed by Au removal using a Au etcher. TCNQ molecules were then thermally evaporated on graphene surfaces. The Au-assisted graphene transfer process can be further applied on the TCNQ layer to add on an additional graphene layer.

be released upon heating/electrical stressing, and they might diffuse to the device active layers, raising reliability concerns. In another related study, the stacked graphene layers were used as the anode for an inverted P3HT/PCBM solar cell structure, where 10 layers of graphene is needed to achieve the PCE of ~2.5%.[44] In this contribution, we developed a layer-by-layer molecular doping process on graphene for forming sandwiched graphene/tetracyanoquinodimethane (TCNQ) stacked films with tunable conductivities as an anode in polymer solar cells. For example, we constructed graphene/TCNQ/graphene, where the TCNQ molecules (p-dopants) were embedded between two graphene layers. In achieving these structures, a Au-assisted graphene transfer process without involving any organic solvent is adopted to avoid the damage or dissolution of TCNQ molecules during the transfer processes. Poly(3-hexylthiophene)/phenyl-C61-butyric acid methyl ester (P3HT/PCBM) bulk heterojunction polymer solar cells based on the multilayered graphene/TCNQ anodes are fabricated and characterized. The anode structure with two TCNQ layers sandwiched by three CVD graphene layers shows the optimum power conversion efficiency of ~2.58%, where stable and low resistance of graphene stacks is achieved without using acid doping. The proposed anode structure may be suitable for next-generation flexible devices requiring high transparency and reliable electrical conductivity.

RESULTS AND DISCUSSION

Au-Assisted and Resist-Free Transfer of Graphene. Large-area monolayer graphene was grown on copper foils at 1000 °C by a CVD method using a mixture of methane and hydrogen gases as reported elsewhere.[45,46] Details are described in the Methods section. All of the as-grown graphene films were characterized by Raman spectroscopy and atomic force microscopy (AFM). The polymer-assisted detachment of CVD graphene from the underlying Cu foils has been reported elsewhere,[26,40,47] in which a layer of poly(methyl methacrylate) (PMMA) was coated on graphene as a supporting layer. After wet-etching of Cu by an aqueous solution containing Fe^{3+} or $S_2O_8^{2-}$ ions, the PMMA-supported graphene films were transferred onto an insulating substrate, followed by PMMA removal with an organic solvent, acetone or chloroform. It is noted that organic solvent is required to remove the unwanted PMMA layer at the final stage of the transfer; hence, this process is not suitable for transferring graphene onto organic thin films. For example, acetone not only removes the PMMA layer above graphene films but also dissolves the organic thin film underlying graphene. Thus, an alternative transfer process without using organic solvents is needed for preparing the layer-by-layer structure of graphene/TCNQ/graphene. A gold film has been used as a supporting layer for the transfer printing of carbon nanotubes,[48,49] where the removal of the supporting Au layer can be performed in an aqueous Au etcher. As schematically illustrated in Figure 1, we have successfully transferred graphene films onto desired substrates using the similar concept. Thirty nanometers of Au was deposited onto the as-grown CVD graphene on a Cu foil. Note that we use thermal evaporation to deposit the Au layer since physical vapor sputtering has been known to damage the graphene layer.[50] The sample was then immersed in an ammonium persulfate solution at 60 °C for 2 h to remove the unwanted Cu foil. After being thoroughly washed, the Au-supported graphene film was fished by a glass substrate. The whole sample was finally immersed in an aqueous gold etcher for 10−20 min, followed by cleaning and drying.

It is known that the as-grown CVD graphene layers on Cu foils exhibit almost no Raman D-band.[46,49] However, the transfer processes involve mechanical strains, solvent treatments, and residue issues, which unavoidably cause structural disorders in graphene. Hence, it is very useful to compare the Au transfer and commonly used PMMA transfer techniques.

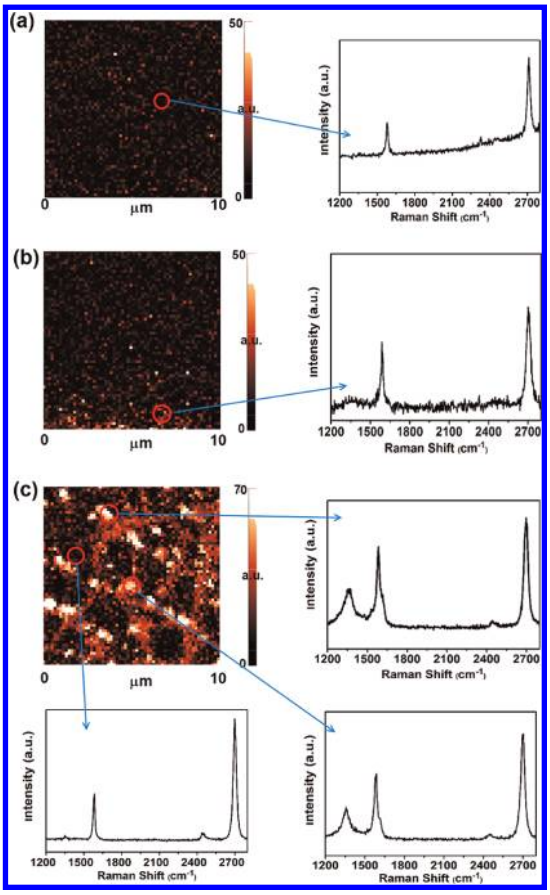

Figure 2. Spatial mappings of Raman D-band for (a) an as-grown CVD graphene on a Cu foil (before transfer), (b) a graphene monolayer transferred onto a glass substrate by the Au transfer method, and (c) a graphene monolayer transferred onto a glass substrate by the PMMA transfer method.

We performed the Raman mapping measurements to examine the quality of the graphene before and after transferring by Au and PMMA, respectively, where the results are shown in Figure 2. We also show the typical sheet resistance, hole mobility, and carrier concentration data for these two graphene films in the Supporting Information Table S1. These characterization results suggest that the D-band was caused by the transfer processes, and the Au transfer process results in a smaller amount of defects in graphene as compared with the PMMA transfer proccess, indicating that the surface of the Au-transferred graphene is cleaner.

Preparation of Graphene/TCNQ Stacked Films. TCNQ or its analogue is known as an efficient p-dopant for carbon nanotubes and graphene[51−54] due to the strong electron deficiency of its aromatic structure. The decoration of graphene surfaces with TCNQ can be achieved by a thermal evaporation method as described in our previous report.[51] In brief, the TCNQ molecules were deposited onto graphene surfaces by gas phase diffusion at 200 °C for 8 h, and TCNQ molecules were allowed to diffuse onto graphene surfaces. The typical thickness of the TCNQ layers deposited on graphene is

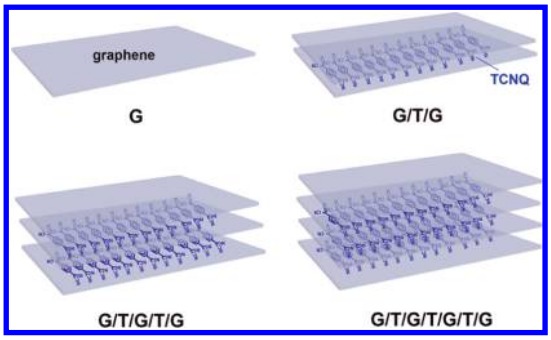

Figure 3. Four anode structures prepared using the methods illustrated in Figure 1. G and T represent a graphene layer and a thermally evaporated TCNQ layer, respectively.

around 2−5 nm using this method, where we show the atomic force microscopy (AFM) results before and after TCNQ decoration for a selected area (Supporting Information Figure S1). Once the first layer of graphene is decorated with TCNQ, a second layer graphene film can be transferred onto the TCNQ layer using the Au-assisted transfer method described above. Since the Au etcher is aqueous, the removal of the Au supporting layer does not cause damage or loss of the TCNQ layer underneath. The graphene transfer and TCNQ decoration processes can be repeated to prepare graphene/TCNQ multilayer stack films. Figure 3 shows the four major anode structures prepared for solar cell device fabrication: (1) G, (2) G/T/G, (3) G/T/G/T/G, and (4) G/T/G/T/G/T/G, where G and T represent graphene and TCNQ layers, respectively.

Characterizations of Graphene/TCNQ Stacked Films. Figure 4a shows the Raman spectra for these films on glass substrates, and the Raman spectra for TCNQ (thick film: several tens of nanometers) are also included for comparison. Note that Raman signals from the TCNQ only several nanometers thick are not detectable in our system. The Raman spectra in Figure 4a demonstrate that both the Raman G and 2D frequencies of graphene upshift once the TCNQ layer is included in the film stacks owing to the hole doping from TCNQ to graphene, agreeing well with previous reports for TCNQ decoration on mechanically exfoliated graphene sheets.[51,54,55] In Supporting Information Figure S2, we show the effect of adding TCNQ on as-grown CVD graphene sheets, where TCNQ molecules induce the Raman G-band shoulder and enhance the baseline signal from ∼1200 to ∼1650 cm^{-1}. The D-band becomes pronouced after TCNQ deposition, indicating that the TCNQ decoration also contributes to the D-band in graphene. This result agrees with the conclusion from our previous report.[55] On the other hand, the low surface roughness of anodes is critically important for avoiding a short circuit between cathodes and anodes. Figure 4b displays the AFM surface topographical images for four types of stacked films, where the surface roughness for these films ranges from 1 to around 2 nm, which is reasonably good for anode applications.

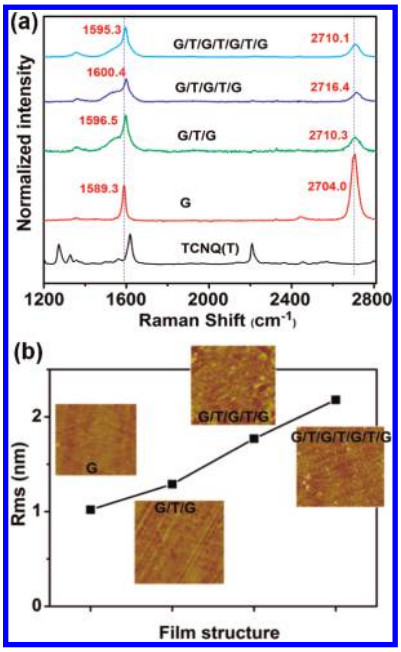

Figure 4. (a) Raman spectra for different graphene/TCNQ stacked films on glass substrates. (b) AFM images and extracted surface roughness values for G, G/T/G, G/T/G/T/G, and G/T/G/T/G/T/G.

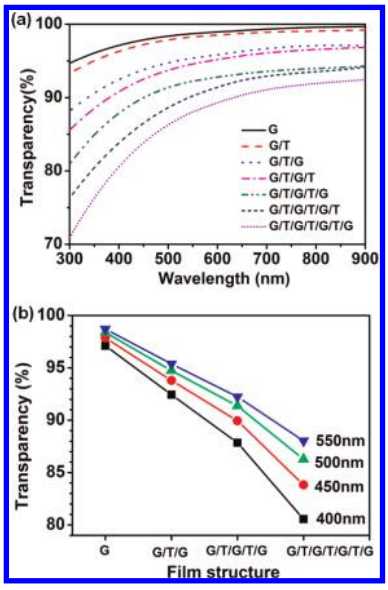

Figure 5. (a) Transparency of various graphene/TCNQ film structures on glass substrates as a function of optical wavelength, where G/T represents the structure TCNQ on graphene. (b) Transparency of four anode structures at various wavelengths (400, 450, 500, and 550 nm). Note that all of the transparency curves have been corrected by a glass substrate baseline.

Figure 5a shows the transparency of various graphene/TCNQ film structures on glass substrates as a function of optical wavelength, where G/T represents the structure TCNQ on graphene. Note these curves have been corrected with a glass substrate baseline. As expected, the transparency decreases with the increasing number of deposited graphene or TCNQ layers. Figure 5b summarizes the transparency of four anode structures at various wavelengths (400, 450, 500, and 550 nm), where the transparency value is ~88% (at 550 nm) even for the thickest G/T/G/T/G/T/G structure.

Figure 6a–c displays the Hall effect measurement results for these four anode films. Hall effect measurements were performed in a homemade system based on Van der Pauw method,[56] and a permanent magnet with 6800 G was used in the system to provide the magnetic field. All of the measurements were taken in ambient conditions for the anode films with a size 1 cm × 1 cm. Figure 6a shows that the sheet resistance of the films monotonically decreases from ~850 Ohm/sq for a monolayer graphene (G) to ~140 Ohm/sq for the G/T/G/T/G/T/G stacked film. The measured hole carrier concentration also monotonically increases from 2.3×10^{13} cm^{-2} for a monolayer graphene to 8.3×10^{13} cm^{-2} for the G/T/G/T/G/T/G film. Moreover, the carrier mobility for the monolayer graphene is significantly lower than that of the graphene/TCNQ stacked film while the mobility value of G/T/G is similar to that of other thicker films. It is known that graphene mobility is severely suppressed by the impurity scattering from underlying substrates;[57–60] thus, the increase in G/T layer thickness likely relieves the scattering effect from substrates and enhances the surface Hall mobility. These results lead to a conclusion that the sheet resistance decrease with G/T layer thickness is mainly due to the hole carrier concentration increase, corroborating that p-doping of TCNQ plays a significant role. More results based on different batches of CVD graphene are shown in the Supporting Information Table S2.

It is noteworthy that the Raman G and 2D peak frequencies in Figure 4a first increase then decrease with the increasing number of graphene layers. One may expect to observe that the Raman G and 2D frequencies for a graphene monolayer should monotonically increase with the carrier concentration.[61–63] Specifically, if we assume all of the carriers are allocated in one graphene layer, one would expect to see a very large G-band shift. For example, the G-band frequency difference between the samples G (carrier concentration ~2.36×10^{13} cm^{-2}) and G/T/G/T/G/T/G (carrier concentration ~8.2×10^{13} cm^{-2}) is expected to be larger than 20 cm^{-1}.[61] However, it should be noted that the carrier concentration obtained from our Hall measurements does not take the number of graphene layers into consideration; in fact, the measured carrier concentration shown in Figure 6a should also include the carriers distributed in the lower graphene layers. Although we believe that the carriers in the deeper layer may have smaller contributions to the measured carrier concentration, we could assume that the measured concentration is close to the total carrier concentration for the time being. On the other hand, the Raman vibration frequencies should reflect the

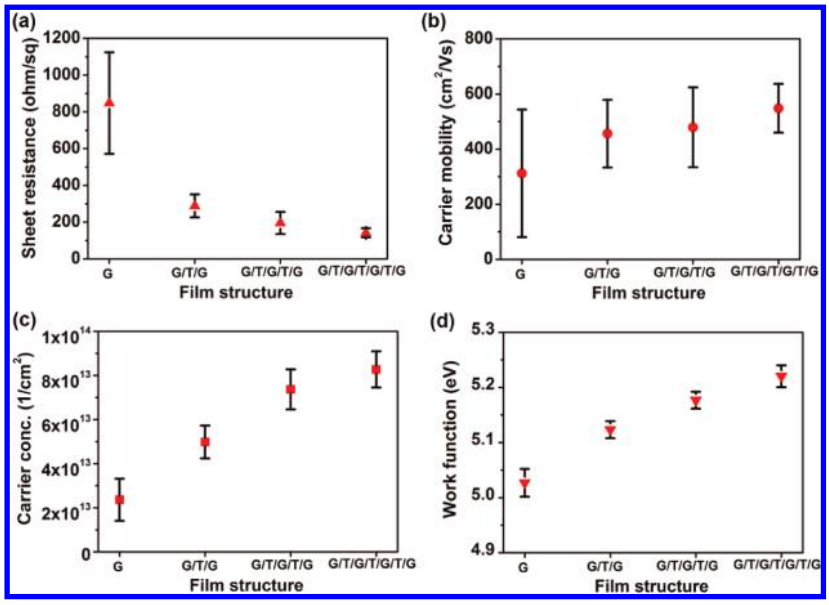

Figure 6. Statistical Hall effect measurement results for these four anode films: (a) sheet resistance, (b) hole carrier mobility, and (c) hole carrier concentration. (d) Work function results based on ultraviolet photoelectron spectroscopy measurement for various graphene/TCNQ stacked films. These statistical measurements were based on 5 to 6 samples for each film structure.

average concentration of the whole stacked graphene films, not the total carrier concentration. After the carrier distribution along the vertical direction was considered simply using the average carrier concentration (measured carrier concentration/number of graphene layers), the carrier concentration displays a better consistent trend with the Raman peak shifts, as shown in the Supporting Information Figure S3. However, it is noted that the average carrier concentration for thicker stacked layers may still be underestimated.

Another important factor worth considering for anode application in polymer solar cells is the work function of the anode. Figure 6d shows the work function values from ultraviolet photoelectron spectroscopy (UPS) measurements for these films. The extracted work function for monolayer graphene is 5.0 eV, and it slightly increases with the G/T layer number up to the 5.2 eV for G/T/G/T/G/T/G. These values match well with the work function of the commonly used hole transporter poly(3,4-ethylenedioxythiophene):poly(styrenesulfonate) (PEDOT:PSS), suggesting that the work function of the G/T stacked films is tunable and suitable for anode applications.

Solar Cell Devices. To study the photovoltaic performance of the invented G/T stacked film anodes, the commonly used P3HT/PCBM blend is chosen as an active layer for bulk heterojunction organic solar cell device fabrication. Figure 7a schematically shows the device structure with G as an anode, where the graphene anode is sitting on a glass substrate and PEDOT:PSS is spun on top of the graphene anode for enhancing hole transport. Ca/Al is used as the reflective cathode. An energy band diagram for the solar cell structure is also plotted in Figure 7a. The measured

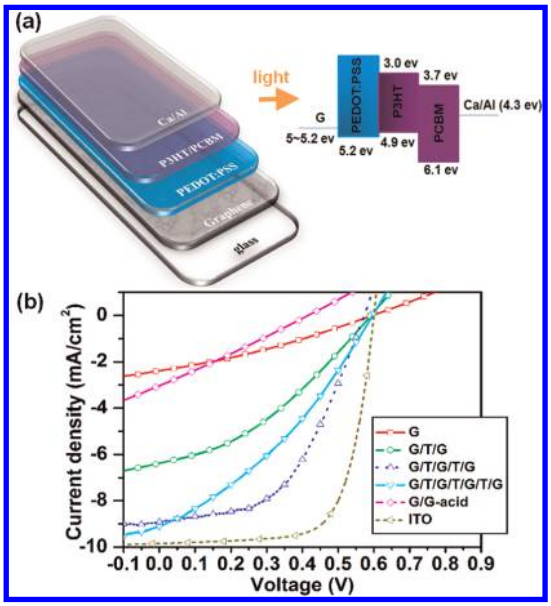

Figure 7. (a) Scheme for the solar cell device with G as an anode, where the graphene anode is sitting on a glass substrate and PEDOT:PSS is spun on top of the graphene anode for enhancing hole transport. Ca/Al is used as the reflective cathode. A band diagram for the solar cell is also shown. (b) Measured current density (*J*)−applied bias (*V*) curves of the fabricated devices as discussed in text.

current density (*J*)−applied bias (*V*) curves of the fabricated devices using various anodes including G, G/T/G, G/T/G/T/G, and G/T/G/T/G/T/G are shown in Figure 7b. For comparison, the photovoltaic performances of devices using ITO and acid-doped bilayer graphene are also included. The curve indicated as G/G-acid in the graph represents the device based on reported acid-doped layer-by-layer graphene electrodes,[43] where the bottom layer graphene is

TABLE 1. Characteristic Photovoltaic Cell Parameters for the Devices Made of Different Anode Films, Including Open Circuit Voltage (V_{OC}), Short Circuit Current Density (J_{SC}), Fill Factor (FF), and Power Conversion Efficiency (PCE)[a]

	sheet resistance (Ohm/sq)	transparency at 550 nm (%)	work function (eV)	V_{OC} (V)	J_{SC} (mA/cm^2)	FF (%)	PCE (%)
G	839	98.7	5.03	0.60	2.39	31.1	0.45
G/T/G	629	95.4	5.13	0.60	6.38	35.7	1.37
G/T/G/T/G	278	92.2	5.18	0.57	8.90	48.0	2.58
G/T/G/T/G/T/G	182	88.0	5.22	0.59	9.10	36.0	1.99
G/G-acid	310	95.0	5.06	0.41	3.03	26.7	0.33
ITO	15	88.0	4.7	0.60	9.85	69.4	4.1

[a] The work function, transparency, and sheet resistance values are also included. Note that the transparency of ITO on glass at 550 nm is 80%, where the glass and ITO absorb 8 and 12%, respectively (Supporting Information Figure S4).

doped with $HCl_{(aq)}$ followed by second layer graphene transfer and then $HNO_{3(aq)}$ doping. Table 1 summarizes the characteristic photovoltaic cell parameters derived from the $J-V$ measurements, including open circuit voltage (V_{OC}), short circuit current density (J_{SC}), filling factor (FF), and PCE for the devices made of these anodes. Note that at least three devices are prepared for each anode, and the data presented are selected from the best for each case. The work function, transparency, and sheet resistance values are also included. The PCE for the device using G anode is ~0.45%, and the PCE increases with the anode G/T layer number up to the 2.58% (for the device using G/T/G/T/G anode). It is noted that the J_{SC} and FF show a similar trend with the G/T layer number. Due to the measured V_{OC} values for the devices made of four anodes being about the same, ~0.57−0.60 V, the enhancement in PCE with G/T layer number seems to correlate well with the decrease in sheet resistance. Further increase in G/T layer number of anode results in a PCE decrease, likely due to the transparency of the anode becoming a limiting factor for the device performance. The device made of the anode G/G-acid exhibits low PCE, FF, and V_{OC} values. One unique feature of this device is its significantly lower V_{OC} (~0.41 V). Acid treatment has been known to be an efficient method to p-dope carbon nanomaterials.[27,41,64−67] However, the acid dopants are easily eliminated by heating or electrical stressing,[68] causing reliability issues in electronic applications. Moreover, for organic electronic devices, the possible acid diffusion to organic layers from acid-doped graphene could also degrade the device performances. It is likely that the acid dopants degrade the interfacial structure of the junction between the anode and active layer.

We observed that the PCE variation for the devices based on G/T/G/T/G/T/G is larger than those on G/T/G/T/G, where we show individual device data in Supporting Information Table S3. Generally, the performance of the devices based on the G/T/G/T/G anode is still consistently better than that based on the G/T/G/T/G/T/G anode. The results in Table 1 suggest that our proposed G/T/G/T/G anode structure exhibits reasonably good performance for organic solar cells. It should be noted that the reference standard cell based on the ITO anode still exhibits the best performance (PCE ~ 4.1%). It is believed that the efforts to improve the conductivity of graphene film, such as better growth techniques and reducing graphene surface impurities, may be the key to further enhancement of the device performance in organic solar cells.

CONCLUSIONS

Au-assisted transfer of graphene to arbitrary substrates has been successfully demonstrated. This transfer process is free of photoresist and without involving organic solvents, which makes it suitable for the transfer of graphene onto organic thin films. Using this transfer process, layer-by-layer graphene/TCNQ stacked films can be obtained. The inclusion of a TCNQ layer significantly increases the hole carrier concentration and decreases the sheet resistance. P3HT/PCBM polymer heterojunction solar cells were fabricated with these highly conductive and transparent graphene/TCNQ anodes. The anode structure with two TCNQ layers sandwiched by three CVD graphene layers shows the optimum PCE of ~2.58%, which makes the invented anode film attractive for next-generation flexible optoelectronic devices demanding high conductivity and transparency.

METHODS

CVD Growth of Graphene. Large-area graphene films were synthesized on copper foil (Alfa Aesar, purity 99.8%; 25 μm thick) by chemical vapor deposition (CVD) in a hot-wall tube furnace. A Cu foil was loaded into the center of the tube, and the system was flushed with a constant flow of hydrogen (415 sccm) at 760 mTorr for 50 min. The Cu foil was annealed at 1000 °C for 40 min to remove organic matter and oxides from the surface. A gas mixture of methane and hydrogen (CH_4 = 60 sccm and H_2 = 15 sccm at 750 mTorr) was introduced into the system at 1000 °C for graphene layer growth. After growth of the graphene films, the graphene/Cu foil was cooled to 25 °C to complete the growth.

Au-Assisted Transfer Process of Graphene. To transfer graphene from a Cu foil to a glass substrate, a thin layer of Au (30 nm) was sputtered on graphene. The Au/graphene/Cu stack film was immersed in an ammonium persulfate solution (Aldrich, 1 M) at 60 °C for 2 h to dissolve Cu foils. The Au-supported graphene

was then thoroughly washed with deionized (DI) water. A glass substrate was used to fish the Au/graphene layers. After hot plate baking at 150 °C for 2 h, the glass substrate with Au/graphene was immersed in a gold etching solution (gold etchant type TFA from Transene Com.; content: iodine complex, potassium iodide, and water) for 10−20 min. Finally, the samples were rinsed with DI water to complete the transfer process.

Preparation of Graphene/TCNQ Stacks. The method to decorate graphene surfaces with tetracyanoquinodimethane (TCNQ; from Aldrich) molecules has been described in our previous report.[51] TCNQ molecules were placed in a vessel that was connected to another vessel with a target substrate (*e.g.*, graphene on glass). These two vessels were initially isolated by a valve and separately pumped to vacuum for 0.5 h to remove the air in the vessels. The setup was then sealed and placed in a preheated oven at 200 °C. Molecules were then allowed to diffuse onto graphene surfaces after switching on the isolation valve. The evaporation period was around 8 h. Once the first layer of graphene film was decorated with TCNQ, the second layer graphene film was then transferred onto it using the Au-assisted transfer method described above. The graphene transfer and TCNQ decoration processes can be multiplied to prepare graphene/TCNQ multilayer stack films. The method to prepare bilayer graphene doped with acid is reported elsewhere.[43] The first layer graphene was doped with HCl (Aldrich, 15 wt %), and then a second layer graphene was transferred on it. The obtained bilayer stack was again doped with HNO_3 (JT Baker, 35 wt %). Note that the graphene was transferred using the Au-assisted transfer method described above.

Solar Cell Devices. The polymer solar cells consisted of a layer of the P3HT/PCBM thin film sandwiched by the graphene-based anode and a metal cathode. The polymer photovoltaic devices were fabricated by spin-coating the P3HT:PCBM blend solution on a PEDOT:PSS coated graphene electrode. Prior to the deposition, a blend of P3HT:PCBM with 1:1 weight ratio was prepared by dissolving it in 1,2-dichlorobenzene with 1:1 weight ratio, followed by stirring the solution for 12 h at 50 °C. It is noted that the PEDOT:PSS layer helps to planarize the graphene surface, to prevent the current leakage and also to aid the hole extraction. We have found that the solar cell devices normally suffer a current leakage issue between graphene electrodes and cathodes if there is no PEDOT:PSS layer on graphene. The active layer was obtained by spin-coating the blend at 600 rpm for 60 s. The active layer was then dried in covered glass Petri dishes. Subsequently, the films were annealed on the top of the hot plate at 130 °C. Thirty nanometers of Ca and 100 nm of Al were sequentially evaporated under vacuum at a pressure below 6×10^{-6} Torr through a shadow mask. The active area of the device was controlled at 0.1 cm^2.

Characterizations. Raman spectra were collected in a NT-MDT confocal Raman microscopic system (laser wavelength = 473 nm and laser spot size $\sim$ 0.5 μm). The Si peak at 520 cm^{-1} was used as reference for wavenumber calibration. The AFM images were performed in a Veeco Dimension-Icon system. The transmittance spectra of the graphene/TCNQ stacks were obtained using a JASCO-V-670 UV−vis spectrophotometer. The sheet resistance, sheet concentration, and mobility of the transparent electrodes were analyzed by using a Hall sensor measurement. UPS spectra were recorded by using an AC-2 photoelectron spectrometer system (Riken Keiki, Japan). Solar cell testing was performed inside a glovebox under simulated AM 1.5G irradiation (100 mW cm^{-2}) by using a Xe lamp-based solar simulator (Thermal Oriel, 1000 W). Electrical characteristics were measured at room temperature under a N_2 environment using an HP 4156C apparatus placed within a glovebox.

Conflict of Interest: The authors declare no competing financial interest.

Acknowledgment. This research was supported by National Science Council Taiwan (NSC-99-2112-M-001-021-MY3 and NSC-100-2120-M-009-006), Nanoproject and Career Development Awards, Academia Sinica. We also acknowledge the strong support from National Chiao Tung University, Taiwan.

Supporting Information Available: AFM images, Raman spectra, Hall measurement, and device results are included. This material is available free of charge *via* the Internet at http://pubs.acs.org.

REFERENCES AND NOTES

1. De Arco, L. G.; Zhang, Y.; Schlenker, C. W.; Ryu, K.; Thompson, M. E.; Zhou, C. W. Continuous, Highly Flexible, and Transparent Graphene Films by Chemical Vapor Deposition for Organic Photovoltaics. *ACS Nano* **2010**, *4*, 2865–2873.
2. Huang, J. H.; Fang, J. H.; Liu, C. C.; Chu, C. W. Effective Work Function Modulation of Graphene/Carbon Nanotube Composite Films as Transparent Cathodes for Organic Optoelectronics. *ACS Nano* **2011**, *5*, 6262–6271.
3. Tung, V. C.; Chen, L. M.; Allen, M. J.; Wassei, J. K.; Nelson, K.; Kaner, R. B.; Yang, Y. Low-Temperature Solution Processing of Graphene-Carbon Nanotube Hybrid Materials for High-Performance Transparent Conductors. *Nano Lett.* **2009**, *9*, 1949–1955.
4. Yin, Z. Y.; Sun, S. Y.; Salim, T.; Wu, S.; Huang, X.; He, Q.; Lam, Y. M.; Zhang, H. Organic Photovoltaic Devices Using Highly Flexible Reduced Graphene Oxide Films as Transparent Electrodes. *ACS Nano* **2010**, *4*, 5263–5268.
5. Tung, V. C.; Huang, J. H.; Tevis, I.; Kim, F.; Kim, J.; Chu, C. W.; Stupp, S. I.; Huang, J. X. Surfactant-Free Water-Processable Photoconductive All-Carbon Composite. *J. Am. Chem. Soc.* **2011**, *133*, 4940–4947.
6. Na, S. I.; Kim, S. S.; Jo, J.; Kim, D. Y. Efficient and Flexible ITO-Free Organic Solar Cells Using Highly Conductive Polymer Anodes. *Adv. Mater.* **2008**, *20*, 4061–4067.
7. Krebs, F. C. All Solution Roll-to-Roll Processed Polymer Solar Cells Free from Indium-Tin-Oxide and Vacuum Coating Steps. *Org. Electron.* **2009**, *10*, 761–768.
8. Yu, G.; Gao, J.; Hummelen, J.; Wudl, F.; Heeger, A. J. Polymer Photovoltaic Cells: Enhanced Efficiencies *via* a Network of Internal Donor−Acceptor Heterojunctions. *Science* **1995**, *270*, 1789–1791.
9. Murray, I. P.; Lou, S. J.; Cote, L. J.; Loser, S.; Kadleck, C. J.; Xu, T.; Szarko, J. M.; Rolczynski, B. S.; Johns, J. E.; Huang, J. X.; *et al.* Graphene Oxide Inter Layers for Robust, High-Efficiency Organic Photovoltaics. *J. Phys. Chem. Lett.* **2011**, *2*, 3006–3012.
10. Kumar, A.; Zhou, C. W. The Race To Replace Tin-Doped Indium Oxide: Which Material Will Win? *ACS Nano* **2010**, *4*, 11–14.
11. Wassei, J. K.; Kaner, R. B. Graphene, a Promising Transparent Conductor. *Mater. Today* **2010**, *13*, 52–59.
12. Zhang, M.; Fang, S. L.; Zakhidov, A. A.; Lee, S. B.; Aliev, A. E.; Williams, C. D.; Atkinson, K. R.; Baughman, R. H. Strong, Transparent, Multifunctional, Carbon Nanotube Sheets. *Science* **2005**, *309*, 1215–1219.
13. Zhang, D. H.; Ryu, K.; Liu, X. L.; Polikarpov, E.; Ly, J.; Tompson, M. E.; Zhou, C. W. Transparent, Conductive, and Flexible Carbon Nanotube Films and Their Application in Organic Light-Emitting Diodes. *Nano Lett.* **2006**, *6*, 1880–1886.
14. Rowell, M. W.; Topinka, M. A.; McGehee, M. D.; Prall, H. J.; Dennler, G.; Sariciftci, N. S.; Hu, L. B.; Gruner, G. Organic Solar Cells with Carbon Nanotube Network Electrodes. *Appl. Phys. Lett.* **2006**, *88*, 233506.
15. Tenent, R. C.; Barnes, T. M.; Bergeson, J. D.; Ferguson, A. J.; To, B.; Gedvilas, L. M.; Heben, M. J.; Blackburn, J. L. Ultrasmooth, Large-Area, High-Uniformity, Conductive Transparent Single-Walled-Carbon-Nanotube Films for Photovoltaics Produced by Ultrasonic Spraying. *Adv. Mater.* **2009**, *21*, 3210–3216.
16. Bertoncello, P.; Edgeworth, J. P.; Macpherson, J. V.; Unwin, P. R. Trace Level Cyclic Voltammetry Facilitated by Single-Walled Carbon Nanotube Network Electrodes. *J. Am. Chem. Soc.* **2007**, *129*, 10982–10983.
17. Lee, J. M.; Park, J. S.; Lee, S. H.; Kim, H.; Yoo, S.; Kim, S. O. Selective Electron- or Hole-Transport Enhancement in Bulk-Heterojunction Organic Solar Cells with N- or B-Doped Carbon Nanotubes. *Adv. Mater.* **2011**, *23*, 629–633.

18. Lee, D. W.; Hong, T. K.; Kang, D.; Lee, J.; Heo, M.; Kim, J. Y.; Kim, B. S.; Shin, H. S. Highly Controllable Transparent and Conducting Thin Films Using Layer-by-Layer Assembly of Oppositely Charged Reduced Graphene Oxides. *J. Mater. Chem.* **2011**, *21*, 3438–3442.
19. Becerril, H. A.; Mao, J.; Liu, Z.; Stoltenberg, R. M.; Bao, Z.; Chen, Y. Evaluation of Solution-Processed Reduced Graphene Oxide Films as Transparent Conductors. *ACS Nano* **2008**, *2*, 463–470.
20. Cote, L. J.; Kim, F.; Huang, J. X. Langmuir−Blodgett Assembly of Graphite Oxide Single Layers. *J. Am. Chem. Soc.* **2009**, *131*, 1043–1049.
21. Yin, Z. Y.; Wu, S. X.; Zhou, X. Z.; Huang, X.; Zhang, Q. C.; Boey, F.; Zhang, H. Electrochemical Deposition of ZnO Nanorods on Transparent Reduced Graphene Oxide Electrodes for Hybrid Solar Cells. *Small* **2010**, *6*, 307–312.
22. Eda, G.; Lin, Y. Y.; Miller, S.; Chen, C. W.; Su, W. F.; Chhowalla, M. Transparent and Conducting Electrodes for Organic Electronics from Reduced Graphene Oxide. *Appl. Phys. Lett.* **2008**, *92*, 233305.
23. Zhao, J. P.; Pei, S. F.; Ren, W. C.; Gao, L. B.; Cheng, H. M. Efficient Preparation of Large-Area Graphene Oxide Sheets for Transparent Conductive Films. *ACS Nano* **2010**, *4*, 5245–5252.
24. Liu, F.; Seo, T. S. A Controllable Self-Assembly Method for Large-Scale Synthesis of Graphene Sponges and Free-Standing Graphene Films. *Adv. Funct. Mater.* **2010**, *20*, 1930–1936.
25. Su, C. Y.; Xu, Y. P.; Zhang, W. J.; Zhao, J. W.; Tang, X. H.; Tsai, C. H.; Li, L. J. Electrical and Spectroscopic Characterizations of Ultra-Large Reduced Graphene Oxide Monolayers. *Chem. Mater.* **2009**, *21*, 5674–5680.
26. Kim, K. S.; Zhao, Y.; Jang, H.; Lee, S. Y.; Kim, J. M.; Kim, K. S.; Ahn, J. H.; Kim, P.; Choi, J. Y.; Hong, B. H. Large-Scale Pattern Growth of Graphene Films for Stretchable Transparent Electrodes. *Nature* **2009**, *457*, 706–710.
27. Bae, S.; Kim, H.; Lee, Y.; Xu, X. F.; Park, J. S.; Zheng, Y.; Balakrishnan, J.; Lei, T.; Kim, H. R.; Song, Y. I.; *et al.* Roll-to-Roll Production of 30-in. Graphene Films for Transparent Electrodes. *Nat. Nanotechnol.* **2010**, *5*, 574–578.
28. Li, X. S.; Zhu, Y. W.; Cai, W. W.; Borysiak, M.; Han, B. Y.; Chen, D.; Piner, R. D.; Colombo, L.; Ruoff, R. S. Transfer of Large-Area Graphene Films for High-Performance Transparent Conductive Electrodes. *Nano Lett.* **2009**, *9*, 4359–4363.
29. Park, H. J.; Meyer, J.; Roth, S.; Skakalova, V. Growth and Properties of Few-Layer Graphene Prepared by Chemical Vapor Deposition. *Carbon* **2010**, *48*, 1088–1094.
30. Shi, Y. M.; Kim, K. K.; Reina, A.; Hofmann, M.; Li, L. J.; Kong, J. Work Function Engineering of Graphene Electrode *via* Chemical Doping. *ACS Nano* **2010**, *4*, 2689–2694.
31. Wu, Y. Q.; Lin, Y. M.; Bol, A. A.; Jenkins, K. A.; Xia, F. N.; Farmer, D. B.; Zhu, Y.; Avouris, P. High-Frequency, Scaled Graphene Transistors on Diamond-like Carbon. *Nature* **2011**, *472*, 74–78.
32. Wei, D. C.; Liu, Y. Q.; Wang, Y.; Zhang, H. L.; Huang, L. P.; Yu, G. Synthesis of N-Doped Graphene by Chemical Vapor Deposition and Its Electrical Properties. *Nano Lett.* **2009**, *9*, 1752–1758.
33. Park, H.; Brown, P. R.; Buloyic, V.; Kong, J. Graphene as Transparent Conducting Electrodes in Organic Photovoltaics: Studies in Graphene Morphology, Hole Transporting Layers, and Counter Electrodes. *Nano Lett.* **2012**, *12*, 133–140.
34. Dong, X. C.; Shi, Y. M.; Huang, W.; Chen, P.; Li, L. J. Electrical Detection of DNA Hybridization with Single-Base Specificity Using Transistors Based on CVD-Grown Graphene Sheets. *Adv. Mater.* **2010**, *22*, 1649–1653.
35. Liu, Y. X.; Dong, X. C.; Chen, P. Biological and Chemical Sensors Based on Graphene Materials. *Chem. Soc. Rev.* **2012**, *41*, 2283–2307.
36. Sinitskii, A.; Tour, J. M. Lithographic Graphitic Memories. *ACS Nano* **2009**, *3*, 2760–2766.
37. Bonaccorso, F.; Sun, Z.; Hasan, T.; Ferrari, A. C. Graphene Photonics and Optoelectronics. *Nat. Photonics* **2010**, *4*, 611–622.
38. Shi, Y. M.; Fang, W. J.; Zhang, K. K.; Zhang, W. J.; Li, L. J. Photoelectrical Response in Single-Layer Graphene Transistors. *Small* **2009**, *5*, 2005–2011.
39. Lian, W. R.; Huang, Y. C.; Liao, Y. A.; Wang, K. L.; Li, L. J.; Su, C. Y.; Liaw, D. J.; Lee, K. R.; Lai, J. Y. Flexible Electrochromic Devices Based on Optoelectronically Active Polynorbornene Layer and Ultratransparent Graphene Electrodes. *Macromolecules* **2011**, *44*, 9550–9555.
40. Kim, K. K.; Reina, A.; Shi, Y. M.; Park, H.; Li, L. J.; Lee, Y. H.; Kong, J. Enhancing the Conductivity of Transparent Graphene Films *via* Doping. *Nanotechnology* **2010**, *21*, 285205.
41. Kasry, A.; Kuroda, M. A.; Martyna, G. J.; Tulevski, G. S.; Bol, A. A. Chemical Doping of Large-Area Stacked Graphene Films for Use as Transparent, Conducting Electrodes. *ACS Nano* **2010**, *4*, 3839–3844.
42. Liu, Z.; Li, J. H.; Sun, Z. H.; Tai, G.; Lau, S. P.; Yan, F. The Application of Highly Doped Single-Layer Graphene as the Top Electrodes of Semitransparent Organic Solar Cells. *ACS Nano* **2012**, *6*, 810–818.
43. Wang, Y.; Tong, S. W.; Xu, X. F.; Ozyilmaz, B.; Loh, K. P. Interface Engineering of Layer-by-Layer Stacked Graphene Anodes for High-Performance Organic Solar Cells. *Adv. Mater.* **2011**, *23*, 1514–1518.
44. Lee, Y.-Y.; Tu, K.-H.; Yu, C.-C.; Li, S.-S.; Hwang, J.-Y.; Lin, C.-C.; Chen, K.-H.; Chen, L.-C.; Chen, H.-L.; Chen, C.-W. Top Laminated Graphene Electrode in a Semitransparent Polymer Solar Cell by Simultaneous Thermal Annealing/Releasing Method. *ACS Nano* **2011**, *5*, 6564–6570.
45. Chen, C. H.; Lin, C. T.; Lee, Y. H.; Liu, K. K.; Su, C. Y.; Zhang, W. J.; Li, L. J. Electrical Probing of Submicroliter Liquid Using Graphene Strip Transistors Built on a Nanopipette. *Small* **2012**, *8*, 43–46.
46. Lu, A. Y.; Wei, S. Y.; Wu, C. Y.; Hernandez, Y.; Chen, T. Y.; Liu, T. H.; Pao, C. W.; Chen, F. R.; Li, L. J.; Juang, Z. Y. Decoupling of CVD Graphene by Controlled Oxidation of Recrystallized Cu. *RSC Adv.* **2012**, *2*, 3008–3013.
47. Reina, A.; Jia, X. T.; Ho, J.; Nezich, D.; Son, H. B.; Bulovic, V.; Dresselhaus, M. S.; Kong, J. Large Area, Few-Layer Graphene Films on Arbitrary Substrates by Chemical Vapor Deposition. *Nano Lett.* **2009**, *9*, 30–35.
48. Kang, S. J.; Kocabas, C.; Kim, H.; Cao, Q.; Meitl, M. A.; Khang, D.; Rogers, J. A. Printed Multilayer Superstructures of Aligned Single-Walled Carbon Nanotubes for Electronic Applications. *Nano Lett.* **2007**, *7*, 3343–3348.
49. Song, L.; Ci, L. J.; Gao, W.; Ajayan, P. M. Transfer Printing of Graphene Using Gold Film. *ACS Nano* **2009**, *3*, 1353–1356.
50. Dimiev, A.; Kosynkin, D. V.; Sinitskii, A.; Slesarev, A.; Sun, Z.; Tour, J. M. Layer-by-Layer Removal of Graphene for Device Patterning. *Science* **2011**, *4*, 1146–1147.
51. Zhang, W. J.; Lin, C. T.; Liu, K. K.; Tite, T.; Su, C. Y.; Chang, C. H.; Lee, Y. H.; Chu, C. W.; Wei, K. H.; Kuo, J. L.; *et al.* Opening Electrical Band Gap of Bilayer Graphene with Molecular Doping. *ACS Nano* **2011**, *5*, 7517–7524.
52. Yuge, R.; Yudasaka, M.; Maigne, A.; Tomonari, M.; Miyawaki, J.; Kubo, Y.; Imai, H.; Ichihashi, T.; Iijima, S. Adsorption Phenomena of Tetracyano-*p*-quinodimethane on Single-Wall Carbon Nanohorns. *J. Phys. Chem. C* **2008**, *112*, 5416–5422.
53. Sun, J. T.; Lu, Y. H.; Chen, W.; Feng, Y. P.; Wee, A. T. S. Linear Tuning of Charge Carriers in Graphene by Organic Molecules and Charge-Transfer Complexes. *Phys. Rev. B* **2010**, *81*, 155403.
54. Hao, R.; Qian, W.; Zhang, L. H.; Hou, Y. L. Aqueous Dispersions of TCNQ-Anion-Stabilized Graphene Sheets. *Chem. Commun.* **2008**, *46*, 6576–6578.
55. Dong, X. C.; Fu, D. L.; Fang, W. J.; Shi, Y. M.; Chen, P.; Li, L. J. Doping Single-Layer Graphene with Aromatic Molecules. *Small* **2009**, *5*, 1422–1426.
56. Van der Pauw, L. J. A Method of Measuring Specific Resistivity and Hall Effect of Discs of Arbitrary Shape. *Philips Tech. Rev.* **1958**, *13*, 1–9.
57. Li, X. S.; Cai, W. W.; An, J. H.; Kim, S.; Nah, J.; Yang, D. X.; Piner, R.; Velamakanni, A.; Jung, I.; Tutuc, E.; *et al.* Large-Area Synthesis of High-Quality and Uniform Graphene Films on Copper Foils. *Science* **2009**, *324*, 1312–1314.

58. Morozov, S. V.; Novoselov, K. S.; Katsnelson, M. I.; Schedin, F.; Elias, D. C.; Jaszczak, J. A.; Geim, A. K. Giant Intrinsic Carrier Mobilities in Graphene and Its Bilayer. *Phys. Rev. Lett.* **2008**, *100*, 016602.
59. Wehling, T. O.; Novoselov, K. S.; Morozov, S. V.; Vdovin, E. E.; Katsnelson, M. I.; Geim, A. K.; Lichtenstein, A. I. Molecular Doping of Graphene. *Nano Lett.* **2008**, *8*, 173–177.
60. Zhang, Y. B.; Tan, Y. W.; Stormer, H. L.; Kim, P. Experimental Observation of the Quantum Hall Effect and Berry's Phase in Graphene. *Nature* **2005**, *438*, 201–204.
61. Das, A.; Pisana, S.; Chakraborty, B.; Piscanec, S.; Saha, S. K.; Waghmare, U. V.; Novoselov, K. S.; Krishnamurthy, H. R.; Geim, A. K.; Ferrari, A. C.; *et al.* Monitoring Dopants by Raman Scattering in An Electrochemically Top-Gated Graphene Transistor. *Nat. Nanotechnol.* **2008**, *3*, 210–215.
62. Lazzeri, M.; Mauri, F. Nonadiabatic Kohn Anomaly in a Doped Graphene Monolayer. *Phys. Rev. Lett.* **2006**, *97*, 266407.
63. Shi, Y. M.; Dong, X. C.; Chen, P.; Wang, J. L.; Li, L. J. Effective Doping of Single-Layer Graphene from Underlying SiO_2 Substrates. *Phys. Rev. B* **2009**, *79*, 115402.
64. Zheng, Q. B.; Gudarzi, M. M.; Wang, S. J.; Geng, Y.; Li, Z. G.; Kim, J. K. Improved Electrical and Optical Characteristics of Transparent Graphene Thin Films Produced by Acid and Doping Treatments. *Carbon* **2011**, *49*, 2905–2916.
65. Zhao, W. J.; Tan, P. H.; Zhang, J.; Liu, J. Charge Transfer and Optical Phonon Mixing in Few-Layer Graphene Chemically Doped with Sulfuric Acid. *Phys. Rev. B* **2010**, *82*, 245423-1-8.
66. Prado, M. C.; Nascimento, R.; Moura, L. G.; Matos, M. J. S.; Mazzoni, M. S. C.; Cancado, L. G.; Chacham, H.; Neves, B. R. A. Two-Dimensional Molecular Crystals of Phosphonic Acids on Graphene. *ACS Nano* **2011**, *5*, 394–398.
67. Zhou, W.; Vavro, J.; Nemes, N. M.; Fischer, J. E.; Borondics, F.; Kamaras, K.; Tanner, D. B. Charge Transfer and Fermi Level Shift in P-Doped Single-Walled Carbon Nanotubes. *Phys. Rev. B* **2005**, *71*, 205423-1-7.
68. Pei, S. F.; Zhao, J. P.; Du, J. H.; Ren, W. C.; Cheng, H. M. Direct Reduction of Graphene Oxide Films into Highly Conductive and Flexible Graphene Films by Hydrohalic Acids. *Carbon* **2010**, *48*, 4466–4474.